

Hardware-Agnostic Modeling of Quantum Side-Channel Leakage via Conditional Dynamics and Learning from Full Correlation Data

Brennan Bell¹, Andreas Trügler^{1,2}, Konstantin Beyer³, Paul Erker^{4,5}

Abstract— We study a sequential coherent side-channel model in which an adversarial probe qubit interacts with a target qubit during a hidden gate sequence. Repeating the same hidden sequence for N shots yields an empirical *full-correlation record*: the joint histogram $\hat{P}_g(b)$ over probe bit-strings $b \in \{0,1\}^k$, which is a sufficient statistic for classical post-processing under identically and independently distributed (i.i.d.) shots but grows exponentially with circuit depth. We first describe this sequential probe framework in a coupling- and measurement-agnostic form, emphasizing the scaling of the observation space and why exact analytic distinguishability becomes intractable with circuit depth.

We then specialize to a representative instantiation (a controlled-rotation probe coupling with fixed projective readout and a commuting R_x gate alphabet) where we (i) derive a depth-dependent leakage envelope whose maximizer predicts a "Goldilocks" coupling band as a function of depth, and (ii) provide an operational decoder, via machine learning, a single parameter-conditioned map from \hat{P}_g to Alice's per-step gate labels, generalizing across coupling and noise settings without retraining. Experiments over broad coupling and noise grids show that strict sequence recovery concentrates near the predicted coupling band and degrades predictably under decoherence and finite-shot estimation.

I. INTRODUCTION

We study a multi-tenant (multi-programmed) quantum processor setting where residual cross-talk creates a side-channel: while Alice executes a depth- k circuit, a nearby adversarial probe qubit (Eve) weakly couples to Alice's register and is repeatedly measured. Eve's measurement statistics leak information about Alice's gate sequence, even though Eve never directly measures Alice's qubits. Such physical implementations can be attacked through e.g. timing and power side-channels, revealing secrets even when the algorithms themselves are cryptographically sound [1], [2]. At scale, micro-architectural leakage [3], [4] and learning-based exploitation [5]–[7] show that weak and noisy signals can become actionable after statistical amplification.

Quantum platforms introduce an additional failure mode: *coherent* leakage. An auxiliary degree of freedom can entangle with an otherwise isolated computation and acquire

phase- and history-dependent signatures that are not well modeled as purely classical noise. This motivates sequential settings where information is transferred repeatedly and then partially erased by measurement back-action and open-system noise [8], [9]. Concretely, Alice applies an unknown length- k gate string on a qubit A , while Eve couples a probe qubit E after each gate and performs mid-circuit measurements on E . Figure 1 summarizes the Alice/Eve interaction and Eve's measurement pipeline. The resulting record is history-dependent: even for fixed coupling strength, statistics at step t depend on the prior gate context through the evolving joint state.

Importantly, *quantum-computing security* has already begun to document practical side-channel surfaces in today's cloud and multi-user stacks. Timing observations in cloud quantum services can leak information about executed workloads and backend selection [10], while power/control-layer observables can reveal pulse-level structure sufficient for circuit reconstruction [11], [12]. In multi-tenant regimes, co-located jobs can interact via device physics (e.g., crosstalk), creating additional attack surfaces [13]. Our focus is complementary: we study a *minimal coherent probe* mechanism that produces a correlation-rich mid-circuit record, and we ask when that record supports *strict sequence recovery* under depth, noise, and shot limits. Here, "depth" means the number of gates in Alice's sequence, i.e. k in $g_{1:k}$ (not circuit depth after compilation). We model Markovian (gate-local, memoryless) noise using quantum channels: after each ideal operation, the state is updated by a completely-positive trace-preserving (CPTP) map \mathcal{N} representing interaction with an environment B , i.e. $\rho \mapsto \mathcal{N}(\rho) = \text{Tr}_B[U(\rho \otimes \sigma_B)U^\dagger]$ [14]. This channel viewpoint [15] cleanly separates coherent unitary evolution from stochastic decoherence and enables contraction-based distinguishability bounds.

A key methodological choice in this paper is a observation model. Rather than restricting Eve to per-step marginals, we allow Eve to retain the *full correlation structure over time*: repeating the *same* hidden sequence of gates for N shots yields an empirical joint histogram $\hat{P}_g(b)$ over probe bit-strings $b \in \{0,1\}^k$. This correlation-rich record is the natural sufficient statistic for classical post-processing under i.i.d. shots, but it is high-dimensional (2^k) and therefore forces explicit representational and inductive-bias choices for learning. Our threat model is motivated by the cross-talk and simultaneous-execution literature on shared quantum hardware, where imperfect isolation can correlate co-scheduled programs and leak information across tenants [13], [16]–[18].

¹ Department of Data Privacy at Know Center GmbH, Graz, Austria. bell.brennan.p@gmail.com

²University of Graz, Graz, Austria. andreas.truegler@uni-graz.at

³Stevens Institute of Technology, Hoboken, NJ, USA. kbeyer1@stevens.edu

⁴Technische Universität Wien, Vienna, Austria.

⁵IQOQI Vienna, Austrian Academy of Sciences, Vienna, Austria. paul.erker@tuwien.ac.at

A. Contributions

General sequential-probe model and observation record. We formalize a sequential coupling-and-measurement threat model and adopt the full-correlation histogram $\hat{P}_g(b)$ as Eve’s sufficient statistic under i.i.d. shots, clarifying the exponential scaling of the observation space and the resulting limits on closed-form distinguishability beyond small depth.

Instantiation-specific analytic predictor (controlled rotations + fixed readout). For a controlled-rotation probe coupling with fixed projective readout and a commuting R_x gate alphabet, we derive a depth-dependent leakage envelope and a closed-form predictor $\theta^*(k)$ for the coupling strength that maximizes distinguishability under repeated interaction. We call the intermediate-leakage regime a *Goldilocks* regime: coupling/noise are neither so small that Eve sees nothing, nor so large that the side-channel becomes either trivial or washed out—yielding maximal learnability in practice.

Amortized decoding from full correlations. Concretely, we train supervised sequence decoders (neural models) to predict gates from Eve’s observed statistics. We evaluate learnability both via information metrics (distribution distinguishability) and via trained decoders that attempt gate-by-gate reconstruction. The decoders are compact and parameter-conditioned, ingesting \hat{P}_g directly (not only marginals) and recovering Alice’s per-step gate labels across coupling and noise grids without retraining per grid point.

II. RELATED WORK AND POSITIONING

Quantum side-channels in cloud stacks. Beyond classical side-channel analysis (SCA), recent work shows that quantum cloud services expose measurable side-channel surfaces tied to the control and execution stack. For example, timing observations on cloud-based quantum services can leak information about the executed workload and service behavior [10]. In addition, power/control-layer side-channels can reveal pulse- and gate-level structure and allow reconstruction of quantum circuits executed on a controller [11], [12]. These results motivate threat models where adversaries exploit *classical* observables that correlate with quantum computation.

Multi-tenant, device-physics-mediated leakage and mitigations. A separate thread studies leakage that arises from shared-hardware physics, especially in multi-tenant (and similarly, in multi-programmed) settings, where co-located jobs may interact through mechanisms such as crosstalk [13], [18], [19]. On the defense side, proposals that reshape effective interaction (e.g., through dynamical decoupling) aim to suppress crosstalk-mediated attacks and reduce information flow through coherent couplings [16], [18]. Together, these lines underscore that quantum side-channel risk is not only a question of classical telemetry, but can also be rooted in coherent, hardware-level interactions.

Our approach: coherent, correlation-rich leakage with an analytic envelope. Unlike existing works that focus on classical telemetry (timing/power) or hardware-level

crosstalk, our work establishes the fundamental limits of sequence learnability when an adversary retains the full temporal correlation structure $\hat{P}_g(b)$.

We focus on a minimal *coherent probe* model: Eve gains information by repeatedly interacting a probe degree of freedom with the computation and measuring mid-circuit, producing a history-dependent record shaped by back-action and open-system contraction [8], [9]. Our main departure from marginal-only analyses is to treat the full-correlation histogram $\hat{P}_g(b)$ as the primitive observation. This ensures that any observed failure of strict recovery can be attributed primarily to *physics* (disturbance, contraction with depth, and finite-shot estimation), rather than to discarded temporal correlations. Unlike prior work that focuses on aggregate performance degradation, we treat cross-talk as an *inference channel* and ask when it enables strict sequence recovery.

III. MODEL AND THREAT SETTING

Noise on Alice is modeled as gate-independent depolarizing noise applied after each timestep: for a single-qubit state ρ , $\mathcal{D}_\lambda(\rho) = (1 - \lambda)\rho + \lambda \mathbb{I}/2$, with λ interpreted as a per-step event rate (Markovian, memoryless). We study how this contraction competes with Eve’s repeated weak coupling.

A. General sequential probe model

Alice’s hidden gate sequence is $g_{1:k} \in \mathcal{G}^k$ with a known alphabet $\mathcal{G} = \{U^{(1)}, \dots, U^{(M)}\}$ acting on a target qubit A . At each step t , Alice applies $U^{(g_t)}$ on A , then A interacts with Eve’s probe E via a fixed two-qubit unitary V (or a parameterized family $V(\vartheta)$), followed by a fixed measurement on E described by a POVM $\{M_y\}_{y \in \{0,1\}}$. Noise is modeled by CPTP maps interleaved at each step (e.g., a channel \mathcal{N}_λ on A and optional readout noise on E). One execution yields a probe bit-string $b = (y_1, \dots, y_k) \in \{0, 1\}^k$ and hence an observation law $P_g(b)$ induced by $(V, \{M_y\}, \mathcal{N}_\lambda)$.

B. Instantiation used in this paper

To obtain concrete, reproducible landscapes, we specialize the general model as follows:

- (i) $V(\theta)$ is a controlled- $R_x(\theta)$ coupling (control on A , target on E);
- (ii) Eve performs a fixed projective Z -measurement on E after each interaction;
- (iii) Eve reinitializes her probe to a fresh state $|0\rangle$ before interacting with Alice’s register;
- (iv) Alice is subject to depolarizing noise \mathcal{N}_λ on A at each step; and
- (v) the gate alphabet is the commuting set $\mathcal{G} = \{R_x(\pi/8), R_x(\pi/2), R_x(\pi)\}$.

The explicit depth-2 “blind spots” and the coupling predictor $\theta^*(k)$ derived in Secs. IV–V are properties of this instantiation; the histogram observation model and scaling arguments apply to the general framework above.

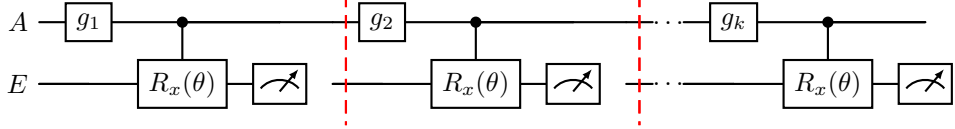


Fig. 1: Sequential coupling protocol: after each hidden gate g_i , Eve couples a probe as $CR_x(\theta)$ and measures it mid-circuit, yielding a probe bit-string over depth k . Repeating N times yields the histogram $\hat{P}_g(b)$.

C. What is (and is not) "hardware-agnostic"

We do not assume a microscopic Hamiltonian for the coupling; instead we treat V (or $V(\vartheta)$) and the measurement $\{M_y\}$ as effective primitives summarizing the interaction and readout in a given protocol. However, learnability *does* depend on the choice of coupling and measurement; changing just Eve's measurement basis generally changes the induced laws and can materially alter strict recovery.

The only invariances we rely on are consistent local re-parameterizations that preserve the induced statistics. For example, for any probe unitary W ,

$$V \mapsto (I \otimes W) V (I \otimes W^\dagger), \quad M_y \mapsto W M_y W^\dagger, \quad (1)$$

leaves $P_g(b)$ unchanged since it corresponds to a basis change on Eve's probe applied consistently to both the coupling and the measurement. Analogous joint conjugations on Alice's side (conjugating both the coupling and the gate alphabet) are statistically equivalent. Outside such consistent transformations, different couplings/measurements correspond to different threat models.

D. Full-correlation observation model

One circuit execution yields a probe bit-string $b = (y_1, \dots, y_k) \in \{0, 1\}^k$. Repeating the *same* hidden sequence for N shots produces counts

$$C(b) = \sum_{i=1}^N \mathbf{1}\{b^{(i)} = b\}, \quad \hat{P}_g(b) = C(b)/N, \quad (2)$$

an empirical distribution on $\{0, 1\}^k$ (dimension 2^k). This is the full-correlation record; per-step marginals are obtained by linear projections of \hat{P}_g and are not assumed as the primary feature.

E. Goal and metrics

Eve aims to infer $g_{1:k}$ from the empirical distribution \hat{P}_g and auxiliary conditioning parameters (coupling θ and noise scale λ). We evaluate: (i) per-position accuracy, and (ii) *strict sequence accuracy* for sequences of length k ,

$$\text{Acc}_{\text{strict}}(d) = \Pr[\hat{g}_{1:k} = g_{1:k}]. \quad (3)$$

IV. INTRACTABILITY AND DEPTH-2 ROOTS IN PAIRWISE DISTINGUISHABILITY

Fix a position t in Alice's sequence. Conditioning on the gate value $g_t \in \{0, 1, 2\}$ partitions random sequences into three classes. For each full sequence g and infinite shots, Eve observes a distribution P_g over her measurement outcomes; we summarize each class by its mean observation law $\bar{P}_{t,a} = \mathbb{E}[P_g \mid g_t = a]$. Any decoder, learned or not, must separate these class means (up to finite-shot estimation noise), so their pairwise distinguishability is a necessary condition for reliable gate recovery at depth t .

The intractability and scaling observations below hold for the general model. The explicit θ -dependent "blind spots" at depth $k = 2$ are derived for the controlled-rotation instantiation in Sec. III-B. A useful way to formalize when strict recovery is even *possible* is to ask whether different hidden sequences induce measurably different laws on Eve's full-correlation record. Fix a sequence length k and write $U_k = g_{1:k} \in \mathcal{G}^k$ for the (unknown) gate sequence. Let $P_g(b)$ denote Eve's *infinite-shot* probe distribution over bit-strings $b \in \{0, 1\}^k$ for a full sequence g , and define the class-conditional *mean* distributions

$$\bar{P}_{k,u}(b) = \mathbb{E}[P_g(b) \mid g_{1:k} = u], \quad u \in \mathcal{G}^k. \quad (4)$$

Any estimator, learned or not, must ultimately separate these class means through the observed finite-shot, multi-nomial estimate \hat{P}_g . Accordingly, we consider a generic pairwise distinguishability functional $D(\cdot, \cdot)$ (e.g., total variation [20], [21], Jensen–Shannon [22], or a smooth proxy [23]) and the induced depth- k separations

$$D_d(u, u') = D(\bar{P}_{d,u}, \bar{P}_{d,u'}), \quad u \neq u'. \quad (5)$$

If $D_d(u, u') = 0$ for some pair, then those two sequences are *information-theoretically indistinguishable* from Eve's record at that (θ, λ) , regardless of shots and decoder.

A. Why analytic distinguishability becomes intractable

The object $\bar{P}_{d,u}$ is an expectation over all length- k continuations consistent with the sequence u . Even in the noiseless case, writing it in closed form entails composing k sequential instruments (unitary coupling + measurement + noise) and averaging over $|\mathcal{G}|^{k-d}$ continuations, while each P_g itself is a distribution on 2^k outcomes. Thus, the exact evaluation of eq. (5) scales exponentially in both depth and outcome dimension (roughly $O(|\mathcal{G}|^{k-d} 2^k)$ for brute-force enumeration), and symbolic expressions rapidly become unwieldy beyond very small k . This motivates (i) envelope-style analytic

proxies that track the dominant informative mode, and (ii) amortized decoders trained directly on \hat{P}_g .

B. Depth-2 roots ("blind spots") in the noiseless case

Depth $k = 2$ is special because Eve's depth-2 observation law is determined by a *two-fold composition of the same measurement instrument* (interaction + selective measurement). As a result, gate-dependence can be summarized by a single scalar *witness* $A_2(\theta; \mathcal{G})$ (e.g., the amplitude of the gate-dependent component in a canonical event probability, or equivalently the coefficient of the leading nontrivial mode in the induced two-step probe channel). For controlled-rotation probe couplings one obtains a factorization of the form

$$A_2(\theta; \mathcal{G}) \propto \sin^2\left(\frac{\theta}{2}\right) \kappa_2(\theta; \mathcal{G}), \quad (6)$$

where $\sin^2(\theta/2)$ is the universal *transfer* pre-factor (vanishing at decoupling angles $\theta \equiv 0 \pmod{2\pi}$), and $\kappa_2(\theta; \mathcal{G})$ is an alphabet-dependent, bounded trigonometric *modulation factor* produced by the *two-step* composition (including measurement back-action).

Crucially, for the coupling family and alphabet used here, κ_2 has isolated zeros. At such couplings θ_0 , the gate-dependent component captured by A_2 vanishes; in our setting this coincides with gate-blindness of the depth-2 probe law, and hence with $D_2(u, u') = 0$ for all $u \neq u'$. Considering the depth-2 sequence, we note that all pairwise separations in eq. (5) vanish:

$$\exists \theta_0 : \kappa_2(\theta_0; \mathcal{G}) = 0 \implies D_2(u, u') = 0 \quad \forall u \neq u' \in \mathcal{G}^2. \quad (7)$$

Intuitively, $\bar{P}_{t,a}$ represents what an observer (Eve) expects to see at position t when the gate a is active, averaged over all other possible gate configurations. For intuition, Fig. 2 visualizes strict prefix recovery at $k = 2$ as a function of (θ, λ, N) , highlighting the trivial failure modes (decoupling and strong noise) and the rapid saturation with shots when distinguishability is present. Operationally, these points appear as "dead zones" in the data. Even in a perfect scenario—with no noise and infinite data—it is impossible to distinguish between different sequences at these specific values (θ_0). This is because the physical patterns the system produces become indistinguishable, meaning the recovery process can do no better than a random guess.

C. From exact roots to envelope-guided ridges

Away from these isolated blind spots, the same mechanism that yields eq. (6) implies that distinguishability grows from zero at weak coupling, peaks at an intermediate "Goldilocks" band, and then is suppressed by repeated interaction and back-action as depth increases. For $d > 2$, one can still track this behavior through a dominant-mode proxy (e.g., eq. (8)) whose maximizer $\theta^*(d)$ predicts the empirical ridge in strict recovery. Noise and finite-shot estimation do not remove the depth-2 roots; they *broaden* them into low-accuracy bands by adding additional contraction and sampling fluctuations on \hat{P}_g .

Note that $\sin^2(\theta/2)$ is π -periodic, whereas $\kappa_2(\theta; \mathcal{G})$ need not be; thus the location (and symmetry) of depth-2 roots is controlled by κ_2 rather than by the universal pre-factor.

V. ENVELOPE-GUIDED COUPLING BAND (FOR CONTROLLED ROTATIONS)

In this section we derive a compact predictor for the coupling ridge for the controlled-rotation instantiation of Sec. III-B; the general sequential-probe framework does not imply a universal $\theta^*(k)$ independent of $(V, \{M_y\})$. This competition produces a characteristic "Goldilocks" regime in θ , where learning is locally maximized across the parameter space: too small yields an undetectable effect at finite shots, too large over-disturbs the dynamics and washes out history-dependent structure.

For controlled-rotation families, a useful analytic proxy is the gate-conditioned spread in a canonical per-step event probability, which can be written (up to an alphabet-dependent scale $\alpha_{\mathcal{G}}$) as

$$\Delta p_k(\theta; \mathcal{G}) \approx \alpha_{\mathcal{G}} \sin^2\left(\frac{\theta}{2}\right) \cos^k\left(\frac{\theta}{2}\right). \quad (8)$$

The $\sin^2(\theta/2)$ factor captures weak-coupling growth of transfer into the probe, while the $\cos^k(\theta/2)$ factor captures depth- k contraction of coherence-like modes under repeated coupling (and, in practice, composes with additional noise-induced contractions).

Maximizing $f_k(\theta) = \sin^2(\theta/2) \cos^k(\theta/2)$ yields the closed-form predictor

$$\theta^*(k) = 2 \arcsin \sqrt{\frac{2}{k+2}}, \quad (9)$$

which shifts to smaller coupling with depth. Operationally, $\theta^*(k)$ predicts where strict recovery should concentrate in coupling sweeps, irrespective of whether Eve uses marginals or full correlations: full correlations can improve sample efficiency, but they cannot move information into regimes where the physical distinguishability is suppressed.

A. Finite-shot floor

The empirical histogram \hat{P}_g is obtained by multi-nomial sampling with N shots, so all distinguishability measures inherit an $O(1/\sqrt{N})$ statistical floor. In particular, when the physically induced spread is below this scale, performance is dominated by sampling fluctuations even if the underlying (infinite-shot) distributions differ.

VI. LEARNING FROM FULL CORRELATION DATA

We learn a single, two-parameter-conditioned decoder

$$f_{\omega} : (\hat{P}_g, \theta, \lambda) \mapsto \hat{g}_{1:k}, \quad (10)$$

trained across a grid of (θ, λ) so that inference is amortized across physical regimes.

Strict prefix accuracy cascade ($k = 2$)

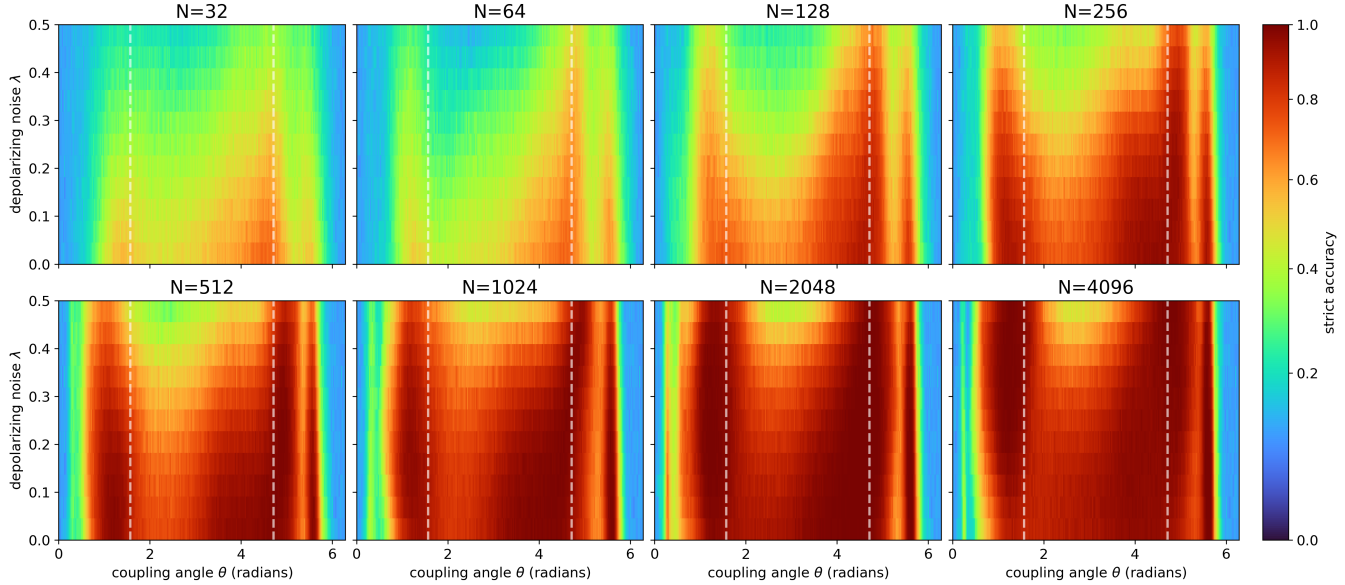


Fig. 2: Strict prefix accuracy cascade for prefix length $k = 2$ over coupling θ and depolarizing noise λ , shown across shots N . This short-depth case serves as a sanity check for the depth-2 analysis in Sec. IV: accuracy collapses at trivial decoupling ($\theta \approx 0, 2\pi$) and under strong noise, and otherwise saturates rapidly with N when distinguishability is present. Dashed lines indicate $\theta^*(2)$ from eq. (9) and its mirror $2\pi - \theta^*(2)$.

A. Histogram-conditioned temporal regressor (Hist-TCN)

Let $x \in \mathbb{R}^{2^k}$ denote the vectorized full-correlation histogram $x = \hat{P}_g(\cdot)$ under a fixed bit-string ordering. We convert x into a length- k feature sequence by repeating it at each time step and appending a positional code and physical conditioning:

$$X_t = [\theta/\pi, \lambda, e_t, x] \in \mathbb{R}^{2+k+2^k}, \quad t = 1, \dots, k, \quad (11)$$

where $e_t \in \{0, 1\}^k$ is the one-hot vector indicating the position t . This yields $X \in \mathbb{R}^{k \times (2+k+2^k)}$, which is processed by a dilated temporal convolutional network (TCN) [24]–[27] over the step index t with a per-step regression head.

The network outputs a scalar $\hat{a}_t \in [0, 1]$ interpreted as a normalized rotation angle $\hat{\varphi}_t/\pi$ at step t . Gate labels are obtained by nearest-neighbor decoding to the known alphabet $\{1/8, 1/2, 1\}$:

$$\hat{g}_t = \arg \min_{m \in \{1/8, 1/2, 1\}} |\hat{a}_t - m|. \quad (12)$$

We train with a smooth ℓ_1 loss on the continuous targets $a_t \in \{1/8, 1/2, 1\}$. Known in the literature as the *Huber* loss [28], the function transitions from quadratic to linear growth beyond a threshold, improving robustness to heavy-tailed errors. This regression formulation is compact and stable under finite-shot noise, and it reuses a single decoder across the full (θ, λ) grid without per-point retraining [29].

We remark that we have also explored Gray-code reorderings [30] and Walsh–Hadamard [31] features for alternative decoders. Here we report Hist-TCN as the strongest compact baseline and refer regarding the further results to future work [32].

B. Why representation matters as dimension scales exponentially

The full-correlation record lives on $\{0, 1\}^k$, and vectorizing it naively imposes an arbitrary geometry on the input. Since 2^k grows quickly (e.g., $k = 15$ gives 32,768 bins), we use representations that expose structure with simple inductive biases: Gray-code ordering makes neighboring indices differ by one bit (useful for local convolution), while the Walsh–Hadamard transform maps the histogram to parity/correlation spectra (useful for multilayer perceptrons (MLPs) with global receptive fields).

C. Conditioning on physical parameters

We concatenate normalized (θ, λ) to the learned embedding before the prediction head. This yields a single amortized decoder that interpolates across the full grid rather than retraining a model per coupling/noise setting.

D. Estimator-independent limit

Information bounds are estimator-agnostic: if the observation laws induced by different sequences become too similar with depth, then *no* decoder can achieve strict recovery. We quantify similarity using total variation $D_{\text{TV}}(P, Q) = \frac{1}{2} \sum_b |P(b) - Q(b)|$ and Kullback–Leibler divergence $D_{\text{KL}}(P \| Q) = \sum_b P(b) \log \frac{P(b)}{Q(b)}$. In our setting, repeated weak coupling plus Markov noise contracts distinguishability with depth, while finite-shot estimation further blurs P_g via multinomial sampling of \hat{P}_g . Standard results (Le Cam/Fano) then lower-bound the achievable error of *any*

Strict prefix accuracy cascade ($k = 7$)

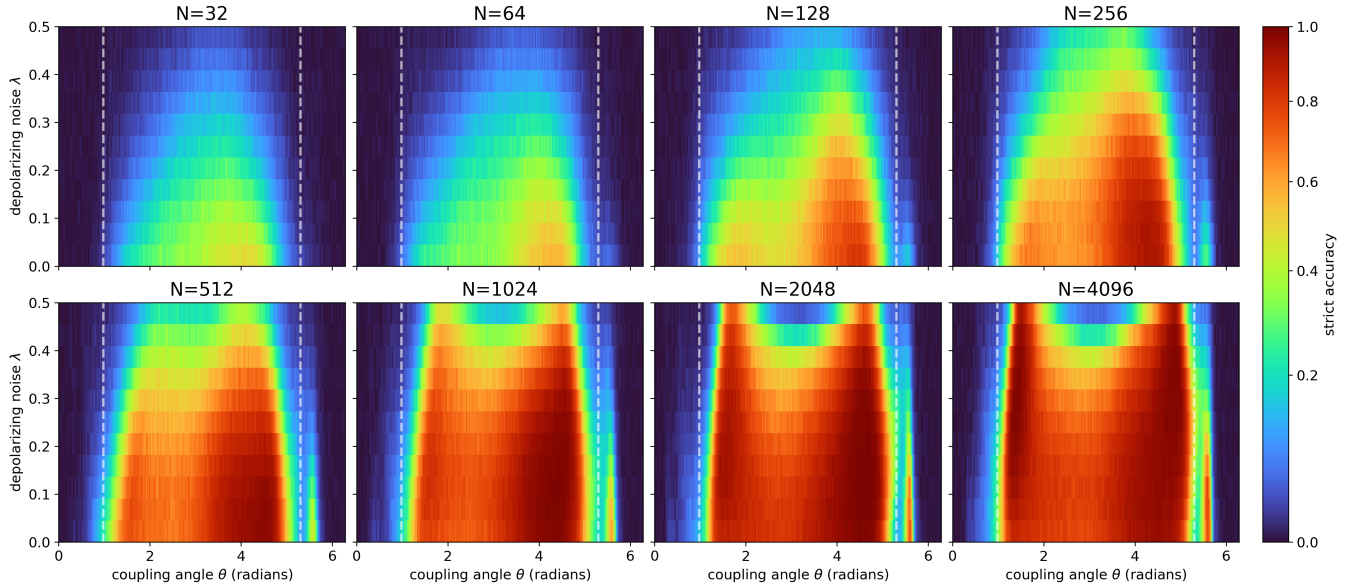


Fig. 3: Strict prefix accuracy cascade for prefix length $k = 7$ over coupling θ and depolarizing noise λ , shown across increasing shots N . The coupling *ridge* (indicated by the vertical dashed lines) is the high-accuracy strength in θ , which tracks the dashed predictor $\theta^*(7)$ from eq. (9) (and the mirrored line $2\pi - \theta^*(7)$, since the proxy is symmetric under $\theta \mapsto 2\pi - \theta$). Noise (y-axis) lowers accuracy and narrows the viable coupling strength as λ increases, while finite-shot effects (indicated by N) represent information density improvements in Eve's data.

estimator in terms of these divergences [33]–[35]. In our setting, repeated coupling and noise contract distinguishability with depth, while finite-shot estimation compounds this via multi-nomial sampling of \widehat{P}_g .

VII. EXPERIMENTAL SETUP

A. Simulation

We simulate two-qubit density-matrix dynamics with interleaved noise and mid-circuit measurement. A typical configuration:

- Gate alphabet $\mathcal{G} = \{\text{Rx}(\pi/8), \text{Rx}(\pi/2), \text{Rx}(\pi)\}$.
- Depth k (e.g., $k = 15$).
- Shots per sequence N (sweep: e.g., $N \in \{32, 64, \dots, 4096\}$).
- Coupling grid $\theta \in [0, 2\pi]$; noise grid λ mapped to a depolarizing rate.

We begin with a commuting alphabet to isolate the effect of sequential interaction and mid-circuit measurement back-action without conflating it with non-commutative control complexity. We choose a commuting R_x alphabet to isolate the effect of repeated probe coupling and Markov noise on learnability and to enable clean analytic envelopes; the side-channel mechanism itself does not rely on commutativity. Extensions to non-commuting alphabets are expected to preserve the same contraction-vs-signal tradeoff but require heavier notation and are left for future work [32]. This choice enables an explicit depth-2 cancellation structure (Sec. IV)

and a simple envelope predictor for the coupling ridge (Sec. V). Extending the study to locally universal alphabets (e.g., including rotations about a second axis) is important future work; we expect the qualitative non-monotone “Goldilocks” phenomenon to persist but with alphabet-dependent modulation and potentially different blind-spot structure.

B. Training and evaluation

Training data are generated by simulating the joint Alice–Eve dynamics for random sequences g , producing Eve's infinite-shot-limit outcome distribution P_g and its finite-shot estimates \widehat{P}_g via multinomial sampling. Inputs to the decoder are either \widehat{P}_g directly or engineered features (such as Gray-code reorderings / Walsh–Hadamard transforms) that improve sample efficiency. We use a TCN because it is stable for long sequences, has a controllable receptive field via dilation, and trains efficiently compared to recurrent baselines. We train a single model across the full (θ, λ) grid with a global train/validation split over sequences. We report strict sequence accuracy heatmaps over (θ, λ) for representative sequence lengths k .

VIII. RESULTS

Figures 2–3 summarize strict prefix accuracy landscapes over coupling θ and depolarizing noise λ as the number of shots N (repetitions of the protocol in Fig. 1) increases across panels. We highlight three phenomena that are directly visible in the cascades and will be referenced throughout.

a) Depth-dependent coupling ridge: In Fig. 3, high-accuracy recovery concentrates in a band in θ (the "ridge") that aligns with the dashed predictor $\theta^*(d)$ from (9) (and its mirror $2\pi - \theta^*(d)$). Comparing $k = 2$ vs. $k = 7$ (Figs. 2 and 3) shows the expected depth trend: the predicted optimal coupling shifts to smaller θ as k increases, and the recoverable region shifts accordingly. In addition, Fig. 2 exhibits narrow low-accuracy bands at specific couplings, consistent with the depth-2 "blind spots" discussed in Sec. IV.

b) Noise narrows the ridge and lowers strict recovery: Holding N fixed and moving upward in λ in Fig. 3 narrows and lowers the ridge: accuracy decreases and the range of viable couplings shrinks. This is consistent with additional channel contraction compounding the depth-dependent suppression in eq. (8).

c) Finite-shot scaling across the cascade: The cascade structure makes the finite-shot effect explicit: for fixed (θ, λ) , moving from smaller to larger N panels increases strict accuracy until it saturates (Figs. 2–3). The largest gains occur near the ridge, where the underlying physics induces distinguishability but small N is still dominated by multinomial sampling fluctuations in \hat{P}_g .

IX. CONCLUSION

Operationally, Eve's side-channel yields gate-level information: in the Goldilocks regime, Eve can predict a nontrivial fraction of Alice's gates (and, depending on parameters, long contiguous subsequences) from passive probe measurements. Outside this regime, contraction with depth and finite-shot noise preclude strict sequence recovery, so the risk is sharply parameter-dependent rather than monotone. Finally, the same coupling that enables leakage can induce back-action on Alice (additional coherent/incoherent error), so characterizing side-channel learnability also informs when co-scheduling causes unacceptable performance degradation for Alice.

Our results support a structured view of coherent leakage under sequential coupling: learnability is not monotone in coupling strength, but concentrates in a depth-dependent band predicted by a simple analytic proxy. Full-correlation records provide additional signal compared to marginals, especially at low shots, but they do not eliminate physical limits imposed by contraction with depth and by multinomial sampling noise. Practically, coherent side-channel risk is therefore best characterized by a landscape over (θ, λ, N, k) rather than a single leakage scalar. In Fig. 3, Eve is *operationally successful* precisely in the ridge region where strict prefix recovery rises well above the random-guess baseline $|\mathcal{G}|^{-d}$ (here $|\mathcal{G}| = 3$) and remains high as N increases; outside this band (or at larger λ), accuracy stays near baseline even with more shots, indicating that the induced observation laws are too contracted to support strict sequence recovery. In practice, Eve is more likely to be successful around the ridge; for θ too far from the optimal ridge lines, additional shots provide little additional information because most distinguishability has been erased already.

ACKNOWLEDGMENTS

An earlier version of this work was presented at the 3rd annual Quantum Computer Cybersecurity Symposium in October 2025; we thank Jakub Szefer for the invitation and further thank the many participants at the symposium for their insights and feedback. BB, AT and PE acknowledge support by the Austrian Federal Ministry of Education, Science, and Research via the Austrian Research Promotion Agency (FFG) through Quantum Austria project QUICHE (No. 914033). KB acknowledges support by the NSF under award No. 2239498, NASA under award No. 80NSSC25K7051 and the Sloan Foundation under award No. G-2023-21102.

REFERENCES

- [1] P. C. Kocher, "Timing attacks on implementations of diffie-hellman, rsa, dss, and other systems," in *Advances in Cryptology – CRYPTO'96*. Berlin, Heidelberg: Springer, 1996, pp. 104–113.
- [2] P. Kocher, J. Jaffe, and B. Jun, "Differential power analysis," in *Advances in Cryptology – CRYPTO'99*. Berlin, Heidelberg: Springer, 1999, pp. 388–397.
- [3] P. Kocher, D. Genkin, D. Gruss, W. Haas, M. Hamburg, M. Lipp, S. Mangard, T. Prescher, M. Schwarz, and Y. Yarom, "Spectre attacks: Exploiting speculative execution," in *Proceedings of the IEEE Symposium on Security and Privacy (SP)*. San Francisco, CA, USA: IEEE, 2019, pp. 1–19.
- [4] M. Lipp, M. Schwarz, D. Gruss, T. Prescher, W. Haas, A. Fogh, J. Horn, S. Mangard, P. Kocher, D. Genkin, and Y. Yarom, "Meltdown," in *Proceedings of the 27th USENIX Security Symposium*. Baltimore, MD, USA: USENIX Association, 2018, pp. 973–990. [Online]. Available: <https://www.usenix.org/conference/usenixsecurity18/presentation/lipp>
- [5] R. Benadjiha, E. Prouff, R. Strullu, E. Cagli, and C. Dumas, "Deep learning for side-channel analysis and profiling," in *IACR Transactions on Cryptographic Hardware and Embedded Systems*, vol. 2018. Gainesville, FL, USA: IACR, 2018, pp. 1–35.
- [6] H. Maghrebi, T. Portigliatti, and E. Prouff, "Deep learning for side-channel analysis: A review," *IEEE Transactions on Information Forensics and Security*, vol. 15, pp. 409–422, 2020.
- [7] I. Goodfellow, Y. Bengio, and A. Courville, *Deep Learning*. Cambridge, MA: MIT Press, 2016. [Online]. Available: <http://www.deeplearningbook.org>
- [8] H.-P. Breuer and F. Petruccione, *The Theory of Open Quantum Systems*. Oxford, UK: Oxford University Press, 2002.
- [9] M. Schlosshauer, *Decoherence and the Quantum-to-Classical Transition*. Berlin, Heidelberg: Springer, 2007.
- [10] C. Lu, E. Telang, A. Aysu, and K. Basu, "Quantum leak: Timing side-channel attacks on cloud-based quantum services," 2024, submitted to IEEE HOST 2024. [Online]. Available: <https://arxiv.org/abs/2401.01521>
- [11] C. Xu, F. Erata, and J. Szefer, "Exploration of quantum computer power side-channels," in *Proceedings of the 2023 ACM Conference on Computer and Communications Security (CCS '23)*. New York, NY, USA: ACM, 2023. [Online]. Available: <https://arxiv.org/abs/2304.03315>
- [12] F. Erata, C. Xu, R. Piskac, and J. Szefer, "Quantum circuit reconstruction from power side-channel attacks on quantum computer controllers," *IACR Transactions on Cryptographic Hardware and Embedded Systems*, vol. 2024, no. 2, pp. 735–768, 2024. [Online]. Available: <https://arxiv.org/abs/2401.15869>
- [13] N. Choudhury, C. Naik Mude, S. Das, P. C. Tikkireddi, S. Tannu, and K. Basu, "Crosstalk-induced side channel threats in multi-tenant NISQ computers," 2024. [Online]. Available: <https://arxiv.org/abs/2412.10507>
- [14] E. Chitambar and G. Gour, "Quantum resource theories," *Reviews of Modern Physics*, vol. 91, no. 2, Apr. 2019. [Online]. Available: <http://dx.doi.org/10.1103/RevModPhys.91.025001>
- [15] T.-R. Jin, Y.-R. Zhang, K. Xu, and H. Fan, "Noisy probabilistic error cancellation and generalized physical implementability," *Communications Physics*, vol. 8, no. 1, p. 296, Jul. 2025. [Online]. Available: <https://doi.org/10.1038/s42005-025-02217-8>

- [16] D. Mehra and A. Kalev, "Defending crosstalk-mediated quantum attacks using dynamical decoupling," 2024. [Online]. Available: <https://arxiv.org/abs/2409.14598>
- [17] S. Maurya, C. N. Mude, B. Lienhard, and S. Tannu, "Understanding side-channel vulnerabilities in superconducting qubit readout architectures," in *2024 IEEE International Conference on Quantum Computing and Engineering (QCE)*, vol. 01, 2024, pp. 1177–1183.
- [18] B. Harper, B. Tonekaboni, B. Goldozian, M. Sevior, and M. Usman, "Crosstalk attacks and defence in a shared quantum computing environment," *Advanced Quantum Technologies*, vol. 8, no. 10, Aug. 2025. [Online]. Available: <http://dx.doi.org/10.1002/qute.202500009>
- [19] X. Yan, C. H. Chang, and T. Zhang, "Defense against ml-based power side-channel attacks on dnn accelerators with adversarial attacks," 2023. [Online]. Available: <https://arxiv.org/abs/2312.04035>
- [20] M.-P. Schützenberger, "Contribution aux applications statistiques de la théorie de l'information," *Publ. Inst. Statist. Univ. Paris*, vol. 3, pp. 3–117, 1954, doctoral thesis, University of Paris, 1953.
- [21] M. S. Pinsker, *Information and Information Stability of Random Variables and Processes*. San Francisco: Holden-Day, 1964, translated and edited by Amiel Feinstein.
- [22] J. Lin, "Divergence measures based on the shannon entropy," *IEEE Transactions on Information Theory*, vol. 37, no. 1, pp. 145–151, 1991.
- [23] M. Cuturi, "Sinkhorn distances: Lightspeed computation of optimal transport," in *Advances in Neural Information Processing Systems 26 (NIPS 2013)*, 2013, pp. 2292–2300. [Online]. Available: <https://papers.nips.cc/paper/4927-sinkhorn-distances-lightspeed-computation-of-optimal-transport.pdf>
- [24] A. Waibel, T. Hanazawa, G. Hinton, K. Shikano, and K. Lang, "Phoneme recognition using time-delay neural networks," *IEEE Transactions on Acoustics, Speech, and Signal Processing*, vol. 37, no. 3, pp. 328–339, 1989.
- [25] C. Lea, M. D. Flynn, R. Vidal, A. Reiter, and G. D. Hager, "Temporal convolutional networks for action segmentation and detection," *CoRR*, vol. abs/1611.05267, 2016. [Online]. Available: <http://arxiv.org/abs/1611.05267>
- [26] S. Bai, J. Z. Kolter, and V. Koltun, "An empirical evaluation of generic convolutional and recurrent networks for sequence modeling," *CoRR*, vol. abs/1803.01271, 2018. [Online]. Available: <http://arxiv.org/abs/1803.01271>
- [27] O. Yazdanbakhsh and S. Dick, "Multivariate time series classification using dilated convolutional neural network," *CoRR*, vol. abs/1905.01697, 2019. [Online]. Available: <http://arxiv.org/abs/1905.01697>
- [28] P. J. Huber, "Robust Estimation of a Location Parameter," *The Annals of Mathematical Statistics*, vol. 35, no. 1, pp. 73 – 101, 1964. [Online]. Available: <https://doi.org/10.1214/aoms/1177703732>
- [29] R. Girshick, "Fast r-cnn," in *Proceedings of the IEEE International Conference on Computer Vision (ICCV)*, December 2015.
- [30] F. Gray, "Pulse code communication," U.S. Patent US2 632 058, March 17, 1953, filed Nov. 1947.
- [31] J. L. Walsh, "A closed set of normal orthogonal functions," *American Journal of Mathematics*, vol. 45, no. 1, pp. 5–24, 1923. [Online]. Available: <https://www.jstor.org/stable/2370258>
- [32] B. Bell, A. Trügler, K. Beyer, and P. Erker, "Hardware-agnostic quantum side-channel attacks," *in preparation*, 2026.
- [33] T. M. Cover and J. A. Thomas, *Elements of Information Theory*, 2nd ed. New York: Wiley, 2006, see Section 2.10 for the finite-hypothesis Fano inequality.
- [34] B. Yu, "Assouad, fano, and le cam," in *Festschrift for Lucien Le Cam: Research Papers in Probability and Statistics*, D. Pollard, E. Torgersen, and G. L. Yang, Eds. New York: Springer, 1997, pp. 423–435.
- [35] A. B. Tsybakov, *Introduction to Nonparametric Estimation*, ser. Springer Series in Statistics. Springer, 2009, revised and extended translation of the 2003 French edition. See Theorem 2.2 (Le Cam) and Theorem 2.5 (Fano) for standard bounds.